

## Article

# Theoretical DFT Investigation of Structure and Electronic Properties of $\eta^5$ -Cyclopentadienyl Half-Sandwich Organochalcogenide Complexes

G. T. Oyeniyi <sup>1</sup> , Iu. A. Melchakova <sup>2</sup>, S. P. Polyutov <sup>3</sup>  and P. V. Avramov <sup>1,\*</sup> 

<sup>1</sup> Department of Chemistry, Kyungpook National University, 80 Daehak-ro, Daegu 41566, Republic of Korea; oyeniyigbenga12@gmail.com

<sup>2</sup> School of Physics and Engineering, ITMO University, St. Petersburg 197101, Russia; iuliia.melchakova@metalab.ifmo.ru

<sup>3</sup> International Research Center of Spectroscopy and Quantum Chemistry (IRC SQC), Siberian Federal University, Svobodny pr. 79/10, 600041 Krasnoyarsk, Russia; polyutov@mail.ru

\* Correspondence: paul.veniaminovich@knu.ac.kr

**Abstract:** For the first time, an extensive theoretical comparative study of the electronic structure and spectra of the  $\eta^5$ -cyclopentadienyl half-sandwich [(Cp)(EPh<sub>3</sub>)], E = Se, Te organochalcogenides was carried out using direct space electronic structure calculations within hybrid, meta, and meta-hybrid DFT GGA functionals coupled with double- $\zeta$  polarized 6-31G\* and correlation-consistent triple-zeta cc-pVTZ-pp basis sets. The absence of covalent bonding between the cyclopentadienyl (Cp) ligands and Te/Se coordination centers was revealed. It was found that the chalcogens are partially positively charged and Cp ligands are partially negatively charged, which directly indicates a visible ionic contribution to Te/Se-Cp chemical bonding. Simulated UV-Vis absorption spectra show that all complexes have a UV-active nature, with a considerable shift in their visible light absorption due to the addition of methyl groups. The highest occupied molecular orbitals exhibit  $\pi$ -bonding between the Te/Se centers and Cp rings, although the majority of the orbital density is localized inside the Cp  $\pi$ -system. The presence of the chalcogen atoms and the extension of  $\pi$ -bonds across the chalcogen-ligand interface make the species promising for advanced photovoltaic and light-emitting applications.

**Keywords:** theoretical chemistry; DFT; TD-DFT; UV-Vis; spectrum; coordination; cyclopentadienyl; chalcogen



**Citation:** Oyeniyi, G.T.; Melchakova, I.A.; Polyutov, S.P.; Avramov, P.V. Theoretical DFT Investigation of Structure and Electronic Properties of  $\eta^5$ -Cyclopentadienyl Half-Sandwich Organochalcogenide Complexes. *Electronics* **2023**, *12*, 2738. <https://doi.org/10.3390/electronics12122738>

Academic Editor: Elena Degoli

Received: 6 May 2023

Revised: 13 June 2023

Accepted: 15 June 2023

Published: 19 June 2023



**Copyright:** © 2023 by the authors. Licensee MDPI, Basel, Switzerland. This article is an open access article distributed under the terms and conditions of the Creative Commons Attribution (CC BY) license (<https://creativecommons.org/licenses/by/4.0/>).

## 1. Introduction

The study of organometallic compounds is a central area of research in inorganic and organic chemistry for many years, with a particular focus on half-sandwich species [1–4]. They are characterized by a metal ion coordinated by two organic ligands and have proven to be of great interest in recent decades due to their potential applications in the fields of catalysis, materials science, and electronics [5–8]. Among the different types, those containing  $\eta^5$ -cyclopentadienyl (Cp) ligands have garnered significant attention, as Cp is known to form stable complexes with transition metals and is a common feature in many industrially relevant catalysts and materials [9–12]. Organochalcogenides containing chalcogen atoms like sulphur, selenium, and tellurium have been found to exhibit a range of unique properties, from being precursors to superconductors [13], optoelectronics [14,15], catalysts [16], and other organometallic compounds [17–20], with potential applications in power transmission, magnetic resonance imaging (MRI), light-emitting diodes (LEDs), photovoltaics, and polymerization processes. They have been shown to exhibit properties such as high thermal stability [21], low thermal expansion [22], and promising optical

properties [19,23], which can be widely utilized as UV-Vis and photoelectrochemical materials [24].

Over time, a significant amount of experimental [25–29] and theoretical work [30–33] has been carried out on  $\eta^5$ -cyclopentadienyl based organochalcogenide complexes. It has been shown that the incorporation of chalcogen coordination centers into complexes leads to a significant change in their bond lengths and angles [25], as well as their electronic properties [34]. The presence of chalcogens has been found to influence the reactivity of the complexes and their suitability for use in catalytic reactions due to their large effective atomic size and diffused electronic clouds, whereas the Cp ligands stabilize the atomic lattice, helping to maintain structural integrity [35]. The recent breakthrough in the experimental synthesis [28] of group 16 elements (selenium, tellurium) forming  $\eta^5$ -cyclopentadienyl half-sandwich complexes incited the extensive theoretical studies necessary for providing perspective on their exploitation. Synthesized from the reaction of  $\text{TeCl}_4$  with benzene in the presence of  $\text{AlCl}_3$ , with  $\text{Ph}_3\text{TeCl}$  as the starting material [28,36], it produces a molecular species with the triphenyl-tellurium moiety  $[\text{Cp}](\text{TePh}_3)$ , followed by an analogous reaction with selenium, achieved from the reaction of  $\text{Ph}_3\text{SeCl}$  with  $\text{LiCp}$  and  $\text{KCp}^{\text{Me}^5}$  [28,37], where the  $\text{Me}^5$  superscript indicates the number of alkyl (methyl) groups attached to the Cp ring.

The absence of chalcogen complexes is particularly puzzling given that their successful synthesis has only recently been achieved. While the Group 13–15 half-sandwich complexes integrating Cp ligands are well known, there is still much to be known about the nature of their chemical reactivity. The ability of chalcogen atoms to form  $\eta^5$ -coordination complexes requires an extensive theoretical study of their optoelectronic properties and chemical reactivity. It is especially important to take into account the unique electronic structure and bonding nature of these complexes, many of which are characterized by strong  $\pi$ -backbonding of organic groups.

In this study, the structural stability and electronic and optical properties of  $\eta^5$ -cyclopentadienyl half-sandwich organochalcogenide complexes ( $[\text{Cp}][(\text{TePh}_3)]$ ,  $[\text{Cp}^{\text{Me}^4}][(\text{TePh}_3)]$ ,  $[\text{Cp}^{\text{Me}^5}][(\text{TePh}_3)]$ ,  $[\text{Cp}][(\text{SePh}_3)]$ , and  $[\text{Cp}^{\text{Me}^5}][(\text{SePh}_3)]$ ) were comparatively studied using electronic structure calculations. The complex interaction energies, the spatial distribution of electron density, the nature of the chemical bonding, and the strength of the chalcogen–ligand bonds were estimated using a set of density functional theory (DFT) hybrid, meta, and hybrid–meta-GGA potentials. Both the TPSS and M06-L meta-GGA functionals demonstrated computational effectiveness in comparison with other DFT approaches. The effects of the addition of methyl groups on the optical properties of the chalcogen complexes were studied to simulate the UV-Vis absorption spectra. It was shown that meta-GGA is suitable for describing the  $\eta^5$ -cyclopentadienyl complexes, addressing the limitations of other functionals, as well as the impact of ligand modifications. The presented theoretical investigation of the stability, reactivity, and electronic structure of these complexes can provide crucial insights and fill the knowledge gaps that would pave the way for the development of new chalcogen-containing compounds. It was shown that Cp ligands induce perturbations of the electronic structure of  $\eta^5$ -coordination chalcogen complexes, which could be promising for a number of quantum, electronic, and optical applications [38–42].

## 2. Computational Methods

To investigate the structure and electronic properties of  $[\text{Cp}](\text{EPh}_3)$  ( $\text{E} = \text{Se}, \text{Te}$ )  $\eta^5$ -cyclopentadienyl half-sandwich organochalcogenide complexes, direct space electronic structure calculations were performed using the density functional theory (DFT) with generalized gradient approximation (DFT-GGA) approach, as implemented in GAMESS software package [43–45] with a convergence criterion of  $10^{-5}$  a.u. Geometry optimizations with C1 symmetry and the energies of the half-sandwich complexes were computed using a set of hybrid (B3LYP [46], PBE0 [47], and B3PW91 [48]), meta (M06-L [49] and TPSS [50]), and hybrid–meta-GGA (M06 [51] and M06-2X [52]) DFT functionals (Table 1). It is well

known that the functionals are successful in reproducing the structures, energies, and electronic properties of organometallic compounds [53–59]. The atomic orbitals of the complexes were described by the polarization-augmented correlation-consistent triple-zeta basis set cc-pVTZ-PP and the double- $\zeta$  polarized 6-31G\*. The effective core potential (ECP), correlation-consistent, and triple-zeta quality in cc-pVTZ-PP for chalcogens decreases the computational cost and provides a better representation of the electron density, which have been used in various studies involving complex systems with intermolecular interactions [53,57,58,60].

**Table 1.** The HOMO–LUMO gaps in eV of  $[\text{Cp}][(\text{EPh}_3)]$  and  $[\text{Cp}][(\text{SePh}_3)]$  complexes were calculated at different levels of the theory. The reliability of seven functionals consisting of hybrid-GGA, meta-GGA, and hybrid-meta-GGA was used to estimate the gap between the highest occupied molecular orbital (HOMO) and the lowest unoccupied molecular orbital (LUMO) gap of the complexes.

| HOMO–LUMO gap(eV)/complex      | Hybrid GGA |       |        | Meta-GGA |       | Hybrid–Meta-GGA |        |
|--------------------------------|------------|-------|--------|----------|-------|-----------------|--------|
|                                | B3LYP      | PBE0  | B3PW91 | M06-L    | TPSS  | M06             | M06-2X |
| $[\text{Cp}][(\text{TePh}_3)]$ | 3.631      | 4.187 | 3.741  | 2.640    | 2.649 | 4.136           | 5.841  |
| $[\text{Cp}][(\text{SePh}_3)]$ | 3.317      | 3.784 | 3.447  | 2.189    | 2.366 | 3.687           | 5.364  |

All five (5)  $\eta^5$ -Cp complexes were designed by connecting the chalcogen (Te/Se) atom to the ligands of three phenyl groups, with Van der Waals  $\eta^5$ -coordination between the cyclopentadienyl and the triphenyl-tellurium/selenium fragment (Figure 1). The background of the initial distances of 2.600 Å between the triphenyl-chalcogen (Te/Se) moiety and the  $\eta^5$ -coordinated cyclopentadienyl ring was obtained from a previous related study of  $\eta^5$ -coordinated cyclopentadienyl complexes [61] coupled with the possibility of adding a number of electrons supplying ( $\text{Me}^4$  and  $\text{Me}^5$ ) alkyl (methyl) groups to the cyclopentadienyl ring subsequently [28,61,62]. The modelling and visualization of the geometries were carried out using Chemcraft software.

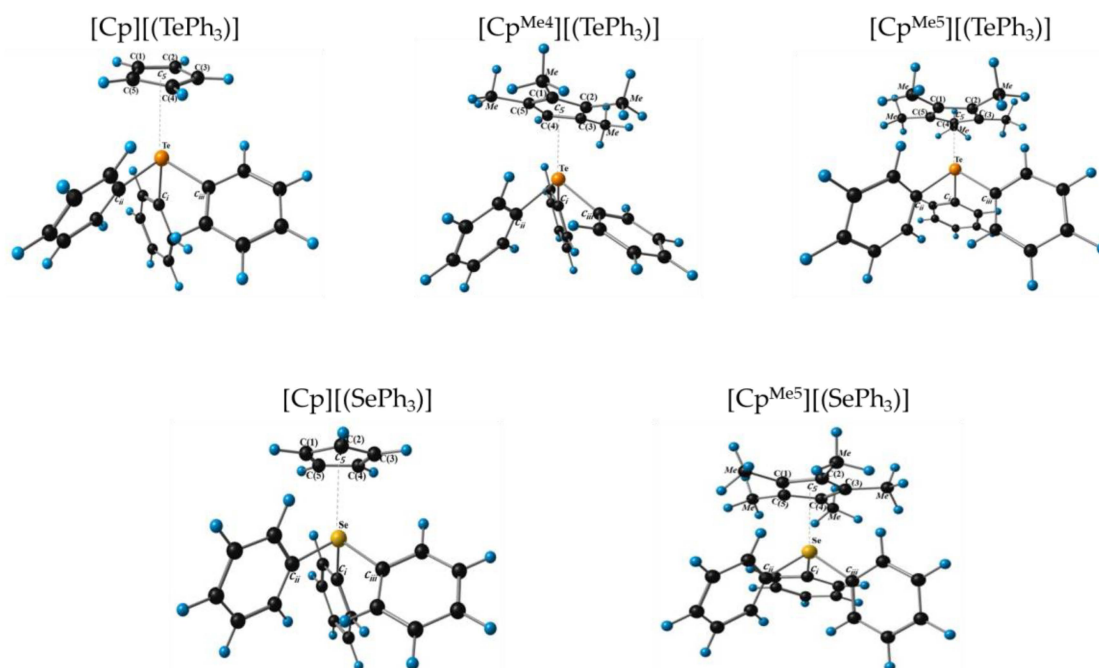


**Figure 1.** The atomic structure of  $[(\text{Cp})(\text{EPh}_3)]$ ,  $\text{E} = \text{Se}, \text{Te}$   $\eta^5$ -Cyclopentadienyl half-sandwich complexes. The hydrogen atoms are depicted in blue, carbon atoms are in black, tellurium atoms are depicted in orange, and selenium atoms are in yellow.

Grimme's D3 dispersion corrections [63,64] were included due to the extended atomic lattices and non-covalent and Van der Waals interactions in the complexes. The vibrational spectrum was also computed to confirm that there was no imaginary frequency, implying that the optimized geometry was a minimum on the potential energy surface. The interaction energies, referred to as complexation energies, were also computed for all complexes [65–67] as follows:

$$\Delta E = E_{F1}(\text{Cp}) + E_{F2}(\text{EPh}_3) - E_P(\text{Cp}(\text{EPh}_3)) \quad (1)$$

where  $\Delta E$  is the complexation energy; and  $E_{F1}$ ,  $E_{F2}$ , and  $E_P$  are the energies of  $\text{Cp}$  (cyclopentadienyl) and  $\text{EPh}_3$  fragments (which are the triphenyl–tellurium/triphenyl–selenium components) for all complexes  $[\text{Cp}][(\text{TePh}_3)]$ ,  $[\text{Cp}^{\text{Me}^4}][(\text{TePh}_3)]$ ,  $[\text{Cp}^{\text{Me}^5}][(\text{TePh}_3)]$ ,  $[\text{Cp}][(\text{SePh}_3)]$ , and  $[\text{Cp}^{\text{Me}^5}][(\text{SePh}_3)]$  (Table S1). The superscripts ( $\text{Me}^4$  and  $\text{Me}^5$ ) on some of the complexes indicate the number of methyl groups attached to the  $\text{Cp}$  ring. The bond length between the connecting carbons in the cyclopentadienyl ( $\text{Cp}$ ) rings ( $\text{C}(1)\sim\text{C}(5)$ ), the distance between each  $\text{Cp}$  carbon atom and the chalcogen atom ( $\text{E}-[\text{C}(1)\sim\text{C}(5)]$ ), the bond length between the chalcogen center and the connecting carbon from the triphenyl ring ( $\text{E}-\text{C}_{i\sim iii}$ )  $\text{C}_{ipso}$ , and the distance from the chalcogen to the center of the  $\text{Cp}$  ring ( $\text{E}-\text{c}_5$ ) were estimated for all complexes, as displayed in Table 2. Time-dependent DFT (TD-DFT) calculations were performed for  $[\text{Cp}][(\text{TePh}_3)]$ ,  $[\text{Cp}^{\text{Me}^4}][(\text{TePh}_3)]$ ,  $[\text{Cp}^{\text{Me}^5}][(\text{TePh}_3)]$ ,  $[\text{Cp}][(\text{SePh}_3)]$ , and  $[\text{Cp}^{\text{Me}^5}][(\text{SePh}_3)]$  complexes to simulate their UV–Vis absorption spectra.

**Table 2.** Structural parameters of five complexes (1, 2, 3, 4 and 5)— $[\text{Cp}][(\text{TePh}_3)]$  (1),  $[\text{Cp}^{\text{Me}^4}][(\text{TePh}_3)]$  (2),  $[\text{Cp}^{\text{Me}^5}][(\text{TePh}_3)]$  (3),  $[\text{Cp}][(\text{SePh}_3)]$  (4), and  $[\text{Cp}^{\text{Me}^5}][(\text{SePh}_3)]$  (5)—obtained at TPSS/(*cc-pVTZ-PP/6-31G\**) in Å and angles in (°); E = Te, Se.

| Complexes  | Distance, C(1)~C(5)                          | Distance, E-[C(1)~C(5)]                       | Distance, E-C <sub>i-iii</sub>                   | Distance, E-c <sub>5</sub>                |
|--|--|---|--|---|
| $[\text{Cp}][(\text{TePh}_3)]$ (1)               | 1.412–1.434                                  | 2.697–3.209                                   | 2.162–2.211                                      | 2.739                                     |
| $[\text{Cp}^{\text{Me}^4}][(\text{TePh}_3)]$ (2) | 1.413–1.438                                  | 2.733–3.123                                   | 2.169–2.218                                      | 2.689                                     |
| $[\text{Cp}^{\text{Me}^5}][(\text{TePh}_3)]$ (3) | 1.417–1.440                                  | 2.764–3.139                                   | 2.157–2.216                                      | 2.702                                     |
| $[\text{Cp}][(\text{SePh}_3)]$ (4)               | 1.417–1.425                                  | 2.854–2.915                                   | 1.982–1.989                                      | 2.602                                     |
| $[\text{Cp}^{\text{Me}^5}][(\text{SePh}_3)]$ (5) | 1.424–1.431                                  | 2.779–2.948                                   | 1.969–2.009                                      | 2.615                                     |
|  | $\angle_{\text{c}_5-\text{E}-\text{c}_i}$    | $\angle_{\text{c}_5-\text{E}-\text{c}_{ii}}$  | $\angle_{\text{c}_5-\text{E}-\text{c}_{iii}}$    | $\angle_{\text{c}_5-\text{E}-\text{c}_3}$ |
| $[\text{Cp}][(\text{TePh}_3)]$ (1)               | 153.127                                      | 108.085                                       | 108.858  | 177.13                                    |
| $[\text{Cp}^{\text{Me}^4}][(\text{TePh}_3)]$ (2) | 148.607                                      | 109.875                                       | 112.531  | 166.76                                    |
| $[\text{Cp}^{\text{Me}^5}][(\text{TePh}_3)]$ (3) | 146.07                                       | 106.45  | 119.33   | 169.45                                    |
| $[\text{Cp}][(\text{SePh}_3)]$ (4)               | 124.74                                       | 118.95  | 120.53   | 177.36                                    |
| $[\text{Cp}^{\text{Me}^5}][(\text{SePh}_3)]$ (5) | 126.393                                      | 113.006                                       | 125.806  | 174.33                                    |
|  | $\angle_{\text{c}_i-\text{E}-\text{c}_{ii}}$ | $\angle_{\text{c}_i-\text{E}-\text{c}_{iii}}$ | $\angle_{\text{c}_{ii}-\text{E}-\text{c}_{iii}}$ |   |
| $[\text{Cp}][(\text{TePh}_3)]$ (1)               | 90.418                                       | 89.209  | 92.022   |   |
| $[\text{Cp}^{\text{Me}^4}][(\text{TePh}_3)]$ (2) | 88.265                                       | 91.821  | 90.940   |   |
| $[\text{Cp}^{\text{Me}^5}][(\text{TePh}_3)]$ (3) | 89.447                                       | 89.604  | 90.310   |   |
| $[\text{Cp}][(\text{SePh}_3)]$ (4)               | 95.03  | 94.80   | 95.94  |   |
| $[\text{Cp}^{\text{Me}^5}][(\text{SePh}_3)]$ (5) | 95.466                                       | 92.440  | 96.429   |   |

### 3. Result and Discussion

#### 3.1. Structure and Stability $\eta^5$ -Cyclopentadienyl Chalcogenide Complexes

The atomic structures of the five  $\eta^5$ -cyclopentadienyl half-sandwich organochalcogenides  $[\text{Cp}][(\text{TePh}_3)]$ ,  $[\text{Cp}^{\text{Me}^4}][(\text{TePh}_3)]$ ,  $[\text{Cp}^{\text{Me}^5}][(\text{TePh}_3)]$ ,  $[\text{Cp}][(\text{SePh}_3)]$ , and  $[\text{Cp}^{\text{Me}^5}][(\text{SePh}_3)]$  are presented in Figure 1 and Table 2. The single-point calculations for all complexes were performed using hybrid, meta, and hybrid–meta-GGA DFT functionals (Table 2). According to Table 1, both hybrid-GGA and hybrid–meta-GGA overestimated the HOMO–LUMO gap of the complexes, which is inconsistent with the results of a recent study using the

TPSS/TZP approach [28]. At TPSS and M06-L (meta-GGA) levels of theory, the HOMO–LUMO gaps for  $[\text{Cp}][(\text{TePh}_3)]$  and  $[\text{Cp}][(\text{SePh}_3)]$  complexes were found to be 2.649/2.640 and 2.366/2.189 eV, respectively, which are close the value obtained in [28]. Although based on the robustness of a larger basis set, the estimated HOMO–LUMO gap obtained in this study at both TPSS/cc-pVTZ-PP and M06-L/cc-pVTZ-PP indicates that it is more precise compared to the data presented in Ref. [28]. Systems with strong intermolecular interactions, such as  $\eta^5$ -Cp organochalcogenide complexes, are not best described by traditional exchange–correlation functionals [68]. They were found to be more adequately described by TPSS and M06-L functionals, which are known to handle systems with non-local exchange–correlation effects, such as chalcogen complexes [69]. This is because the two meta-GGA functionals (TPSS and M06-L) provide a comprehensive treatment of the electron density, which enables a better description of these intermolecular interactions and a more precise prediction of the energy gap of these complexes.

The structural parameters of all five organochalcogenides complexes bound in  $\eta^5$ -coordination with cyclopentadienyl were optimized, as shown in Figure 1, with the atomic coordinates presented in SI. The Cp ring for the  $[\text{Cp}][(\text{TePh}_3)]$  complex was distorted around the rotation axis, with the carbon bond lengths ranging between 1.412 and 1.434 Å (Table 2). There was a slight increase in the bond length of the carbon ring in Cp for all complexes, for example, from 1.434 Å for complex 1 to 1.438 Å for complex 2. It can be seen that complex 1  $[\text{Cp}][(\text{TePh}_3)]$  outcomes are strikingly similar to those obtained for complexes 2  $[\text{Cp}^{\text{Me}4}][(\text{TePh}_3)]$  and 3  $[\text{Cp}^{\text{Me}5}][(\text{TePh}_3)]$  (Table 2). All three tellurium-containing complexes have relatively large Te-centroid ( $\text{Te-c}_5$ ) distances of 2.739, 2.689, and 2.702 Å, respectively.

The donor capability of a  $\text{CH}_3$ -group shows that electron density would be transferred to the Cp ring, and the more H atoms that are substituted by methyls, the more obvious the effect. Also, because Te is more metallic than Se, a greater migration of electron density to Te than to the Se region is expected. The metallic properties are known to increase or become stronger in the group (O, S, Se, Te), which should also make the bonding stronger as the  $\text{CH}_3$ -group is introduced (Figure 2). The higher electronegativity of the Se atom (2.55) in comparison with Te atom (2.10) leads to a shorter E-c5 bond length (Table 2 and Figure 2) and higher complexation energies (Table 3). The difference in the electronegativity of Te/Se could also lead to a decrease in the atomic charge, which could cause the donor capability of the  $\text{CH}_3$ -group towards the Cp ring, combined with the higher electronegativity of selenium. This decrease can be facilitated by the strong sigma donation from the methyl groups, which effectively repels the charge transfer, causing the Te-centroid to be a little more than the Se-centroid.

**Table 3.** Complexation energy  $\Delta E$  (kcal/mol) of  $[(\text{Cp})(\text{EPh}_3)]$ , E = Se, Te) and its derivatives,  $\eta^5$ -distance (Å), HOMO–LUMO gap  $E_g$  (eV), ionization potential IP (eV), electron affinity EA (eV), and dipole moment D (Debye) obtained at the TPSS/cc-pVTZ-PP/6-31G\* level of theory.

| Complexes                                   | $\Delta E$ | $\eta^5$ -Distance | $E_g$ | IP   | EA   | Dipole Moment |
|---|------------|--------------------|-------|------|------|---------------|
| $[\text{Cp}][(\text{TePh}_3)]$              | −59.93     | 2.74               | 2.65  | 4.27 | 1.62 | 4.74          |
| $[\text{Cp}^{\text{Me}4}][(\text{TePh}_3)]$ | −55.95     | 2.69               | 2.42  | 3.96 | 1.54 | 3.71          |
| $[\text{Cp}^{\text{Me}5}][(\text{TePh}_3)]$ | −55.17     | 2.70               | 2.25  | 3.84 | 1.56 | 3.44          |
| $[\text{Cp}][(\text{SePh}_3)]$              | −62.90     | 2.60               | 2.37  | 3.93 | 1.56 | 6.23          |
| $[\text{Cp}^{\text{Me}5}][(\text{SePh}_3)]$ | −58.16     | 2.62               | 1.98  | 3.55 | 1.57 | 4.92          |

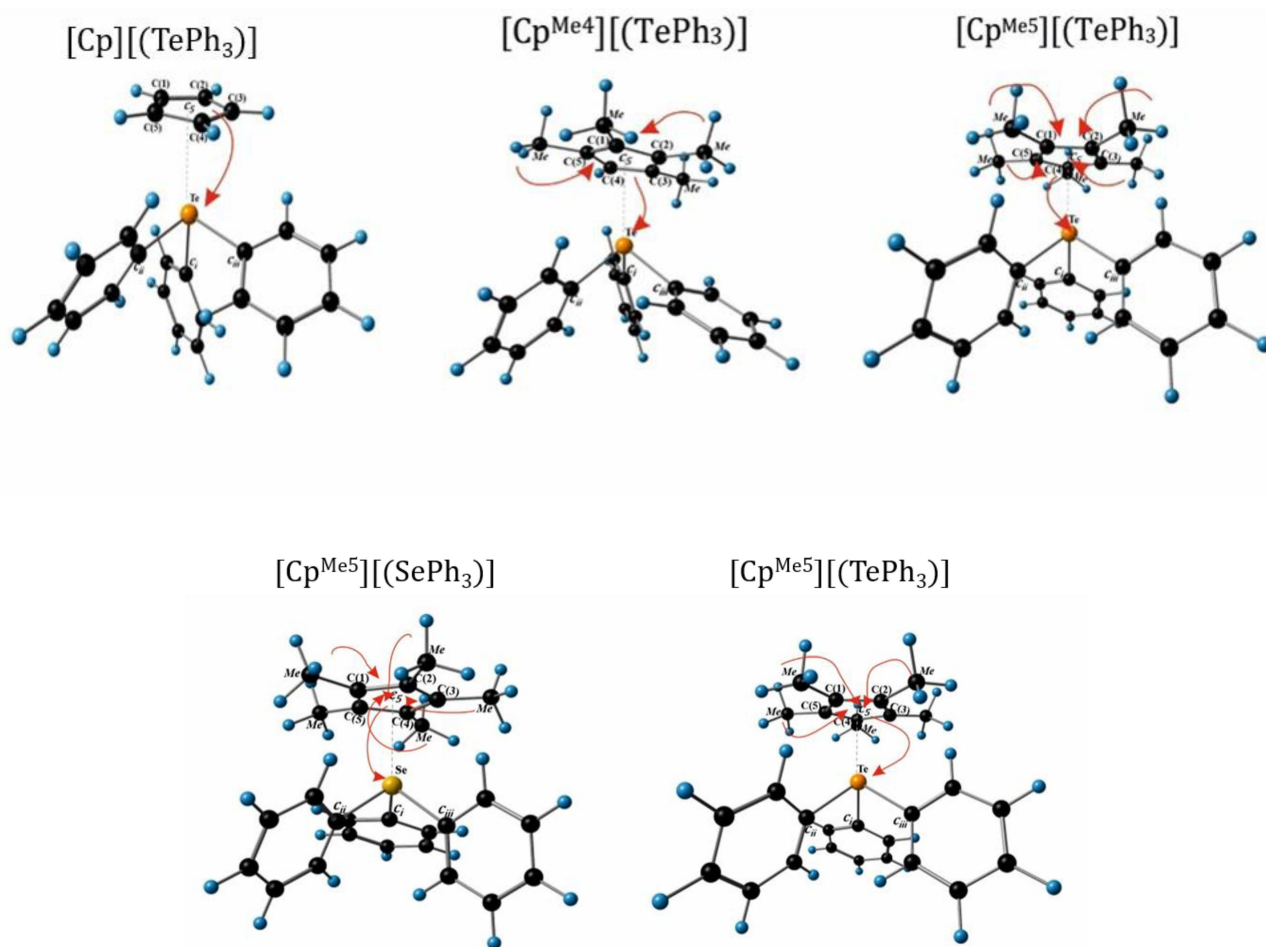


**Figure 2.** Chalcogen bonding interactions between complexes 1 and 3 and comparison between complexes 3 and 5.

The Te-centroids for  $[\text{Cp}^{\text{Me}4}][(\text{TePh}_3)]$  and  $[\text{Cp}^{\text{Me}5}][(\text{TePh}_3)]$  (Table 2) are slightly reduced when more electro-rich methyl groups are added to the cyclopentadienyl fragments. It was observed that the sandwiched and half-sandwich complexes of  $[\text{Cp}^{\text{Me}4}][(\text{TePh}_3)]$  and  $[\text{Cp}^{\text{Me}5}][(\text{TePh}_3)]$  exhibit bent or deformed geometries, indicating that the  $\eta^5$  coordination is not entirely symmetrical when viewed from the center of the  $\text{C}_p$  ring (Figure 1). The distortion from perfectly symmetric coordination is also noticeable when comparing the angle between the  $\text{C}_p$  centroid and the midpoint of the carbon atoms from the  $[\text{TePh}_3]$  fragment. This is also noticeable in the changes in the electron density localization from the  $\text{C}_p$  ring as a methyl group is added. The angle between the  $\text{C}_p$ -centroid and the mid-point between the  $\text{C}_{ipso}$  atoms, ( $\angle_{\text{C}_5-\text{E}-\text{C}_3}$ ), for  $[\text{Cp}][(\text{TePh}_3)]$ ,  $[\text{Cp}^{\text{Me}4}][(\text{TePh}_3)]$ , and  $[\text{Cp}^{\text{Me}5}][(\text{TePh}_3)]$  were observed to be  $177.13^\circ$ ,  $166.76^\circ$ ,  $169.45^\circ$ , respectively; with  $177.36^\circ$  and  $174.33^\circ$  for  $[\text{Cp}][(\text{SePh}_3)]$  and  $[\text{Cp}^{\text{Me}5}][(\text{SePh}_3)]$ , respectively. The loss of perfect symmetry in  $\angle_{\text{C}_5-\text{E}-\text{C}_3}$  is visible, which can be ascribed to the distortion within the complexes due to steric hindrance. This possibly arises from repulsive interactions between the chalcogen center and the  $\text{C}_p$  ring. These interactions occurred due to the overlap of electron clouds, and the chalcogen center hinders a close approach to the  $\text{C}_p$  ring that is responsible for affecting the shape and structure of the complexes but is also important in stabilizing the  $\text{C}_p$  ring in the complex [70,71].

The coordination of the  $\text{C}_p$  rings leaves the  $[\text{TePh}_3]$  moiety mostly unaltered. As shown in Table 2,  $\text{Te}-\text{C}_i \sim \text{Te}-\text{C}_{iii}$  ranges between 2.162–2.211, 2.169–2.218, and 2.157–2.216 Å for complexes  $[\text{Cp}][(\text{TePh}_3)]$ ,  $[\text{Cp}^{\text{Me}4}][(\text{TePh}_3)]$ , and  $[\text{Cp}^{\text{Me}5}][(\text{TePh}_3)]$ , respectively. The variance in the  $\text{C}_{ipso}-\text{Te}-\text{C}_{ipso}$  angles,  $\angle_{\text{C}_i-\text{E}-\text{C}_{ii}}$ ,  $\angle_{\text{C}_i-\text{E}-\text{C}_{iii}}$ , and  $\angle_{\text{C}_{ii}-\text{E}-\text{C}_{iii}}$  within and between

the complexes ( $[\text{Cp}][(\text{TePh}_3)]$ ,  $[\text{Cp}^{\text{Me}4}][(\text{TePh}_3)]$ , and  $[\text{Cp}^{\text{Me}5}][(\text{TePh}_3)]$ ) are similar, with an average of  $90.55^\circ$ ,  $90.34^\circ$ , and  $89.79^\circ$  for complexes  $[\text{Cp}][(\text{TePh}_3)]$ ,  $[\text{Cp}^{\text{Me}4}][(\text{TePh}_3)]$  and  $[\text{Cp}^{\text{Me}5}][(\text{TePh}_3)]$ , respectively. The distance between the Te atom and each of the carbon atoms of the  $\text{C}_p$  ring changes significantly, which ranges between 2.697 and 3.209, 2.733 and 3.123, and 2.764 and 3.139 Å for complexes ( $[\text{Cp}][(\text{TePh}_3)]$ ,  $[\text{Cp}^{\text{Me}4}][(\text{TePh}_3)]$ , and  $[\text{Cp}^{\text{Me}5}][(\text{TePh}_3)]$ , respectively. The structural parameters demonstrate a close agreement with a recent study on similar complexes [28]. It is seen in the case of the addition of an alkyl (methyl) group to the  $\text{C}_p$  ring in the selenium-containing complex that it increases the angle in  $c_5\text{-E-}c_i$  and  $c_5\text{-E-}c_{iii}$ , with a decrease in  $c_5\text{-E-}c_{ii}$ . It is seen that the chalcogen-carbon bond length slightly increases upon the addition of the  $\text{C}_p$  ring, coupled with a slightly decreased angle of  $c\text{-Te-c}$  from  $90^\circ$  for complexes  $[\text{Cp}^{\text{Me}4}][(\text{TePh}_3)]$  and  $[\text{Cp}^{\text{Me}5}][(\text{TePh}_3)]$  as the  $\text{C}_p$  ring becomes more electron-rich. The differences can be observed by comparing the tellurium ( $[\text{Cp}][(\text{TePh}_3)]$ ,  $[\text{Cp}^{\text{Me}4}][(\text{TePh}_3)]$ , and  $[\text{Cp}^{\text{Me}5}][(\text{TePh}_3)]$ ) and selenium ( $[\text{Cp}][(\text{SePh}_3)]$  and  $[\text{Cp}^{\text{Me}5}][(\text{SePh}_3)]$ ), which demonstrate shortened  $\text{E-C}_{i-iii}$  bond lengths in the latter case from an average of 2.187 Å for  $[\text{Cp}][(\text{TePh}_3)]$  to 1.986 Å for  $[\text{Cp}][(\text{SePh}_3)]$ . This may be due to the differences in Van der Waals radii between tellurium and selenium where  $\Delta r_{\text{vdW}}$  is 0.2 Å [72,73]. The chalcogen centroids ( $\text{E-}c_5$ ) demonstrate small differences between the Te and Se complexes, which were observed to be 2.739 Å for  $[\text{Cp}][(\text{TePh}_3)]$ , 2.602 Å for  $[\text{Cp}][(\text{SePh}_3)]$ , 2.702 Å for  $[\text{Cp}^{\text{Me}5}][(\text{TePh}_3)]$ , and 2.615 Å for  $[\text{Cp}^{\text{Me}5}][(\text{SePh}_3)]$ . The distance observed for both Te-centroid and Se-centroid ( $\text{E-}c_5$ ) for all complexes suggest a non-covalent and weakened intermolecular interaction; however, the electrostatic attraction also suggests an ionic interaction, which mostly arises from the electronegativity difference between the chalcogens (Te/Se) and the Cp ligand.

The complexation energies (Table 3) were computed for  $[\text{Cp}][(\text{TePh}_3)]$ ,  $[\text{Cp}^{\text{Me}4}][(\text{TePh}_3)]$ ,  $[\text{Cp}^{\text{Me}5}][(\text{TePh}_3)]$ ,  $[\text{Cp}][(\text{SePh}_3)]$ , and  $[\text{Cp}^{\text{Me}5}][(\text{SePh}_3)]$  complexes. At the TPSS level of theory,  $\Delta E$  is  $-59.93$ ,  $-55.95$ ,  $-55.17$ ,  $-62.90$ , and  $-58.16$  kcal/mole, respectively.  $[\text{Cp}][(\text{SePh}_3)]$ , for which  $\Delta E$  is  $-62.90$  kcal/mol, has the strongest interaction, whereas  $[\text{Cp}^{\text{Me}5}][(\text{TePh}_3)]$  ( $\Delta E = -55.17$  kcal/mol) has the weakest one. The addition of an electron-rich group to the moiety increases the complexation energy for both tellurium ( $-59.93 < -55.95 < -55.17$ ) and selenium ( $-62.90 < -58.16$ ) complexes, which is attributed to the increase in the electron density around the cyclopentadienyl ring, leading to stronger electrostatic interactions with the chalcogen center.

The complexation energies estimated to be from  $-62.90$  to  $-55.17$  kcal/mol imply that the complexes could be chemically stable, as a significant amount of energy is needed for the dissociation. However, among the five complexes,  $[\text{Cp}][(\text{SePh}_3)]$  complex demonstrates the highest stability caused by the deepest  $\Delta E = -62.90$  kcal/mol, with  $[\text{Cp}^{\text{Me}5}][(\text{TePh}_3)]$  showing the least stability with  $\Delta E = -55.17$  kcal/mol.

### 3.2. Electronic Structure of $\eta^5$ -Cyclopentadienyl Organochalcogenide Complexes

The TPSS/(cc-pVTZ-PP/6-31G\*) level of theory was considered over M06-L due to its computational efficiency and transferability. It is seen that  $[\text{Cp}][(\text{TePh}_3)]$ ,  $[\text{Cp}^{\text{Me}4}][(\text{TePh}_3)]$ ,  $[\text{Cp}^{\text{Me}5}][(\text{TePh}_3)]$ ,  $[\text{Cp}][(\text{SePh}_3)]$ , and  $[\text{Cp}^{\text{Me}5}][(\text{SePh}_3)]$  complexes demonstrate distinctive differences in their electronic structure with medium semiconducting HOMO-LUMO energy gaps within the visible optical spectrum 1.98–2.65 eV (Table 3). A significant decrease in the HOMO-LUMO gap can be observed for both  $[\text{Cp}^{\text{Me}4}][(\text{TePh}_3)]$  and  $[\text{Cp}^{\text{Me}5}][(\text{TePh}_3)]$  at the same level of theory, which can be attributed to the electron-rich group added to the cyclopentadienyl ring coupled with the tilted ring. Similarly, for both selenium complexes ( $[\text{Cp}][(\text{SePh}_3)]$  and  $[\text{Cp}^{\text{Me}5}][(\text{SePh}_3)]$ ), the HOMO-LUMO shrinks from 2.37 to 1.98 eV. The decrease in their HOMO-LUMO gap may increase the chemical reactivity [74], although stability may decrease with increased chemical reactivity, which could make both  $[\text{Cp}][(\text{TePh}_3)]$  and  $[\text{Cp}][(\text{SePh}_3)]$  more stable than their derivatives [75]. The extent to which the atomic orbitals overlap influences the HOMO-LUMO gap for both complexes. The stronger complexation energy in  $[\text{Cp}][(\text{SePh}_3)]$  symbolizes greater overlap, which results in a smaller HOMO-LUMO gap. The degree of overlap is determined by the distance

between the atoms; the closer they are, the stronger the bonding and the greater the degree of overlap.

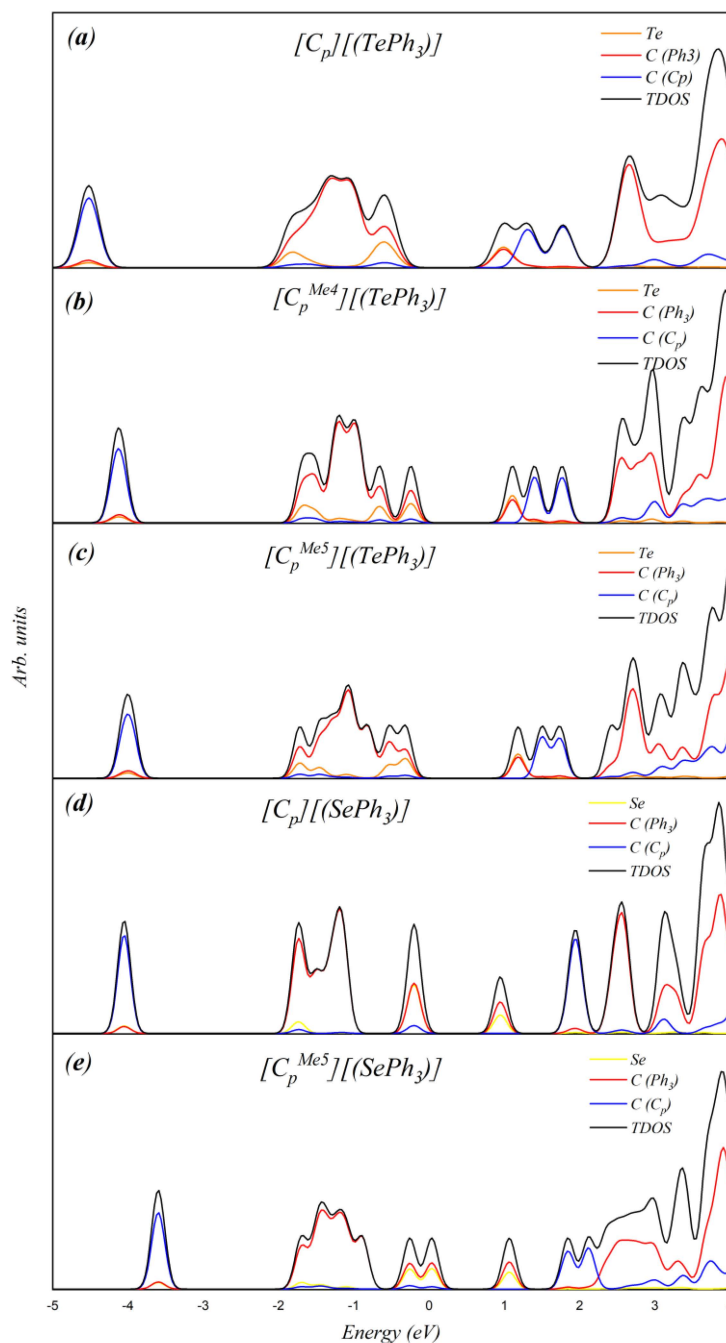
The stability of  $\eta^5$ -cyclopentadienyl complexes can also be considered in terms of their ionization potentials (IP) and electron affinities (EA) (Table 3). The electron-rich methyl groups added to the  $C_p$  ring decrease the IP for both the tellurium and selenium complexes in the range of 4.27–3.84 to 3.93–3.55 eV, respectively, making  $[Cp][TePh_3]$  complex more stable than  $[Cp^{Me^4}][TePh_3]$  and  $[Cp^{Me^5}][TePh_3]$  complexes. The  $[Cp][SePh_3]$  complex is more stable than  $[Cp^{Me^5}][SePh_3]$  one. However, the electronic affinity for  $[Cp][TePh_3]$ ,  $[Cp^{Me^4}][TePh_3]$ , and  $[Cp^{Me^5}][TePh_3]$  complexes decreases in the range of 1.62–1.54 eV, which could cause slightly higher chemical reactivity in the last two complexes.

The separation of electrical charges within the complexes can be measured by the dipole moments (Table 3), which can be used to determine the ionic character of the chemical bonding. It is seen that complex 1 is moderately polar with a dipole moment of 4.74D. The complexes are promising for photovoltaic applications due to their polar character, which may facilitate charge separation [76] and transport properties [77], and remarkable catalytic activity for reactions involving polar intermediates or transition states [78]. The dipole moments of the tellurium-containing complexes are seen to decrease as more electrons are supplied to the  $C_p$  ring, i.e.,  $4.74 > 3.71 > 3.44$  D.  $[Cp][SePh_3]$  with a dipole moment of 6.23 D shows a higher value than all the tellurium complexes, including the dipole moment (4.92 D) of  $[Cp^{Me^5}][SePh_3]$ . The polarity of all tellurium-containing complexes decreases upon the addition of electron-rich methyl groups to the  $C_p$  ring, indicating a lesser ionic character and a larger covalent contribution. The lower dipole moment of  $[Cp^{Me^5}][TePh_3]$  (3.44D) shows that it is relatively nonpolar with primarily covalent chemical bonding. The higher dipole moment of 6.231 D of  $[Cp][SePh_3]$  indicates a high degree of polarity and a more ionic character in comparison with the other complexes. That is, the order of their ( $[Cp][TePh_3]$ ,  $[Cp^{Me^4}][TePh_3]$ ,  $[Cp^{Me^5}][TePh_3]$ ,  $[Cp][SePh_3]$ , and  $[Cp^{Me^5}][SePh_3]$ ) increasing the ionic character from the dipole moment values is  $3.442 < 3.707 < 4.741 < 4.921 < 6.231$  D (Table 3). This order is similar to the order of complexation energies, with complex 4 having the highest complexation energy ( $-62.90$  kcal mol $^{-1}$ ). The highest dipole moment (6 D) and highest complexation energy ( $-62.90$  kcal mol $^{-1}$ ) can be ascribed to a larger electronegativity difference, thereby favouring a more ionic character in the metal–ligand bond. The presence of higher ionic character in the metal–ligand bond enhances electrostatic interactions, resulting in a stronger complexation energy, which signifies a more stable complex and is predicted to exhibit potential superior catalytic activity via an enhanced reactivity mechanism [79–81].

Figure 3a–e and Table 4 show the partial density of states (PDOS), the total density of states (TDOS), and the spatial electron density distributions of the HOMO and LUMO states of  $[Cp][TePh_3]$ ,  $[Cp^{Me^4}][TePh_3]$ ,  $[Cp^{Me^5}][TePh_3]$ ,  $[Cp][SePh_3]$ , and  $[Cp^{Me^5}][SePh_3]$ . It can be observed for  $[Cp][TePh_3]$ ,  $[Cp^{Me^4}][TePh_3]$ , and  $[Cp^{Me^5}][TePh_3]$  that the HOMO states are localized at the carbon atom from the cyclopentadienyl ( $C_p$ ) ring, while the LUMO states are localized at the triphenyl ( $Ph_3$ ) fragments connected to the tellurium atom. The HOMO and LUMO states localized on the  $C_p$  ring and the  $TePh_3$  fragments, respectively, point to either their electron acceptor or the electron donor abilities. Similarly, the HOMO and LUMO states of  $[Cp][SePh_3]$  and  $[Cp^{Me^5}][SePh_3]$  are also found to be localized at the electron-rich  $C_p$  ring with a little contribution from the selenium atom without a significant contribution from  $Ph_3$  to the HOMO states.

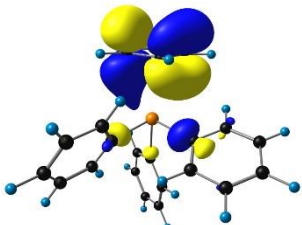
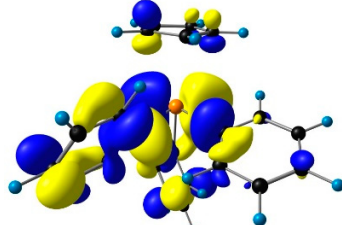
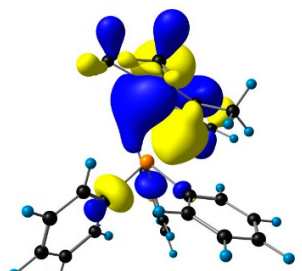
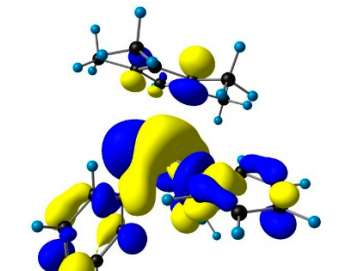
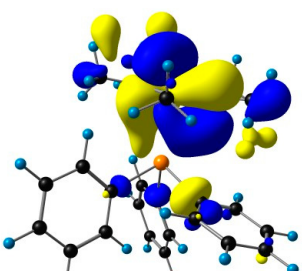
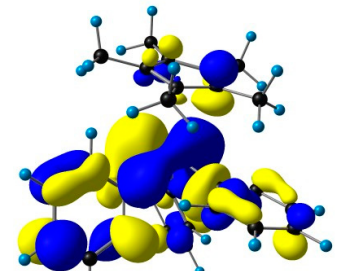
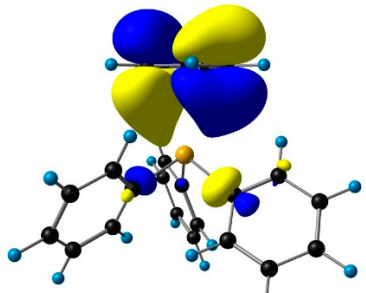
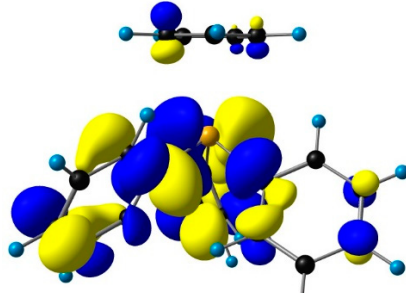
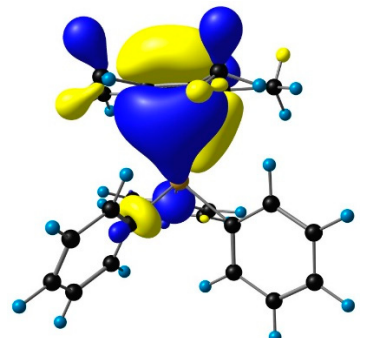
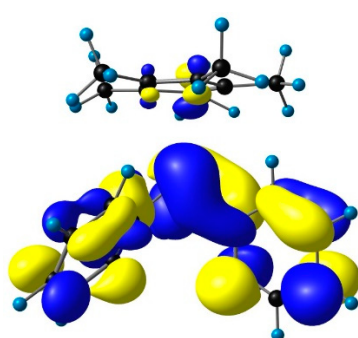
The total and partial density of states (Figure 3) of the tellurium complexes demonstrate that the major contribution to the LUMO comes from the carbon atoms from  $Ph_3$  with visible percentages (25%, 21%, and 20%) from the tellurium atom of  $[Cp][TePh_3]$ ,  $[Cp^{Me^4}][TePh_3]$ , and  $[Cp^{Me^5}][TePh_3]$ , respectively. The HOMO states can be seen to have a significant contribution from the carbon atoms from  $C_p$  rings (blue lines) coupled with a major contribution from the phenyl carbon atoms (Figure 3), which is in good agreement with the analysis of HOMO and LUMO isosurfaces in Table 4. On the other hand, the selenium atom shows little or no contribution to the LUMO states of  $[Cp][SePh_3]$  and

$[\text{Cp}^{\text{Me5}}][\text{SePh}_3]$  (Table 4), with Cp maintaining its contribution to the HOMO state in all five complexes.



**Figure 3.** Total and partial density of states of (a)  $[\text{Cp}][\text{TePh}_3]$ , (b)  $[\text{Cp}^{\text{Me4}}][\text{TePh}_3]$ , (c)  $[\text{Cp}^{\text{Me5}}][\text{TePh}_3]$ , (d)  $[\text{Cp}][\text{SePh}_3]$ , and (e)  $[\text{Cp}^{\text{Me5}}][\text{SePh}_3]$  calculated at TPSS/cc-pVTZ-PP/6–31G<sup>+</sup> level of theory. The tellurium atom is depicted in the orange line, the selenium atom in yellow, the triphenyl carbon atoms in red, the cyclopentadienyl (Cp) carbon atoms in blue, and the total density of state (TDOS) in black.

**Table 4.** Isosurfaces of HOMO and LUMO states calculated for the complexes ([Cp][TePh<sub>3</sub>]), [Cp<sup>Me4</sup>][TePh<sub>3</sub>], [Cp<sup>Me5</sup>][TePh<sub>3</sub>], [Cp][SePh<sub>3</sub>], and [Cp<sup>Me5</sup>][SePh<sub>3</sub>]). Blue represents the positive phase of the wave function and yellow represents the negative phase of the wave function.

| Complexes                                | HOMO  | LUMO  |
|--|---|---|
| [Cp][TePh <sub>3</sub> ]                 |    |    |
| [Cp <sup>Me4</sup> ][TePh <sub>3</sub> ] |    |    |
| [Cp <sup>Me5</sup> ][TePh <sub>3</sub> ] |  |  |
| [Cp][SePh <sub>3</sub> ]                 |  |  |
| [Cp <sup>Me5</sup> ][SePh <sub>3</sub> ] |  |  |

In order to study the nature of the electronic transitions of the organochalcogenide complexes and their derivatives upon the addition of the electron-rich groups to the stabilized Cp ring, TD-DFT TPSS/cc-pVTZ-PP/6-31G\* calculations were carried out for all the complexes ( $[C_p][TePh_3]$ ,  $[C_p^{Me_4}][TePh_3]$ ,  $[C_p^{Me_5}][TePh_3]$ ,  $[C_p][SePh_3]$ , and  $[C_p^{Me_5}][SePh_3]$ ), based on their optimized molecular structures to simulate their UV-Vis absorption spectra. The absorption spectra are shown in different colours for the five complexes:  $[C_p][TePh_3]$  in purple,  $[C_p^{Me_4}][TePh_3]$  in blue,  $[C_p^{Me_5}][TePh_3]$  in red,  $[C_p][SePh_3]$  in brown, and  $[C_p^{Me_5}][SePh_3]$  in yellow in Figure 4. It was found that the wavelength absorption peaks vary with a change in the compositions originating from the addition of methyl to the Cp ring, with 358 nm, 400 nm, 406 nm, 421 nm, and 462 nm for  $[C_p][TePh_3]$ ,  $[C_p^{Me_4}][TePh_3]$ ,  $[C_p^{Me_5}][TePh_3]$ ,  $[C_p][SePh_3]$ , and  $[C_p^{Me_5}][SePh_3]$ , respectively. It can be seen that the absorption wavelength position for the absorption peak for  $[C_p][TePh_3]$  falls within the ultraviolet spectral region, whereas the energy positions of the absorption peaks for  $[C_p^{Me_4}][TePh_3]$ ,  $[C_p^{Me_5}][TePh_3]$ ,  $[C_p][SePh_3]$ , and  $[C_p^{Me_5}][SePh_3]$  have visibly longer wavelengths equal to 400, 406, 421, and 462 nm, respectively, which belong to the visible spectral range. The optical absorption at the visible range is consistent with its band gap values (2.42, 2.25, 2.37, and 1.98 eV) for  $[C_p^{Me_4}][TePh_3]$ ,  $[C_p^{Me_5}][TePh_3]$ ,  $[C_p][SePh_3]$ , and  $[C_p^{Me_5}][SePh_3]$ , respectively. On the other hand, the wavelength absorption peak for  $[C_p][TePh_3]$  and band gap of 2.65 eV can efficiently absorb high-energy UV light, generating a large number of electron-hole pairs that could exhibit strong photoconductivity [82]. It is seen from the spectra that the addition of the methyl groups to the complexes leads to a considerable shift in their visible light absorption, which converts the tellurium-containing complexes from the ultraviolet active region to the visible purple, blue, and red spectral regions for  $[C_p][TePh_3]$ ,  $[C_p^{Me_4}][TePh_3]$ , and  $[C_p^{Me_5}][TePh_3]$ , respectively. This is due to the alteration of the nature of the orbitals upon the addition of the methyl groups and the increase in their ligand field strength, as observed in their complexation energies.

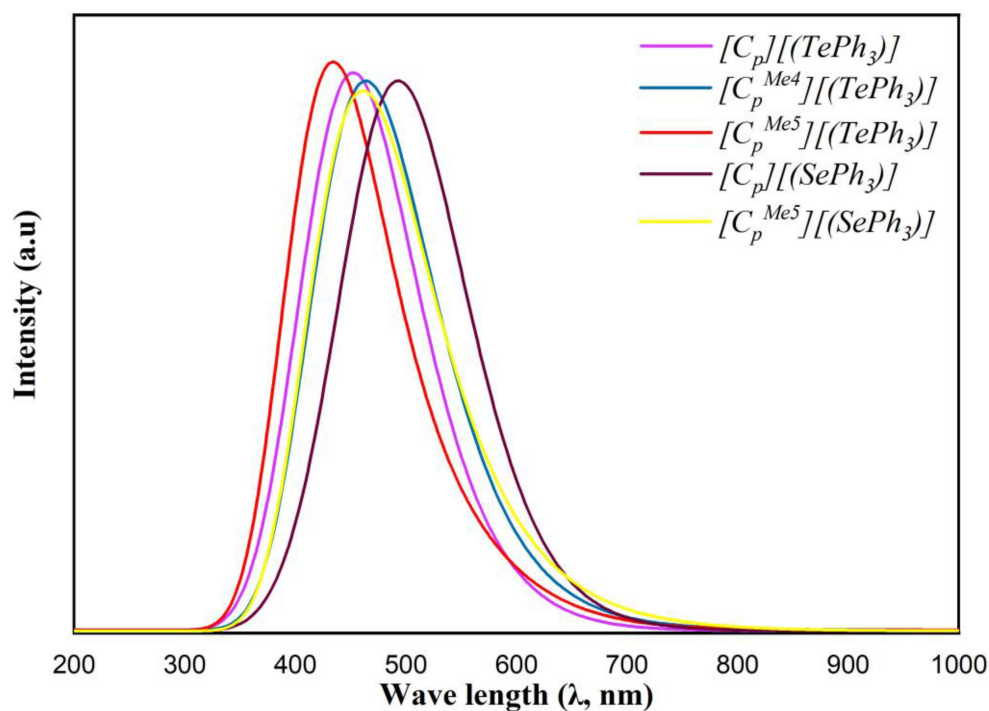


**Figure 4.** Absorption spectra of the complexes at TPSS/cc-pVTZ-PP/6-31G\* level of theory for  $[C_p][TePh_3]$  (purple),  $[C_p^{Me_4}][TePh_3]$  (blue),  $[C_p^{Me_5}][TePh_3]$  (red),  $[C_p][SePh_3]$  (brown), and  $[C_p^{Me_5}][SePh_3]$  (yellow).

#### 4. Conclusions

The atomic and electronic structures and absorption spectra of  $\eta^5$ -cyclopentadienyl half-sandwich organochalcogenides ( $[\text{Cp}][(\text{TePh}_3)]$ ,  $[\text{Cp}^{\text{Me}4}][(\text{TePh}_3)]$ ,  $[\text{Cp}^{\text{Me}5}][(\text{TePh}_3)]$ ,  $[\text{Cp}][(\text{SePh}_3)]$ , and  $[\text{Cp}^{\text{Me}5}][(\text{SePh}_3)]$ ) were characterized using DFT TPSS/cc-pVTZ-PP/6-31G\* electronic structure calculations. It was found that hybrid, meta, and hybrid–meta-GGA DFT functionals overestimate the complexes' HOMO–LUMO energy gaps, with only meta-GGA (TPSS and M06-L) providing a precise estimation coupled with the robustness of the double- $\zeta$  polarized 6-31G\* and correlation-consistent triple-zeta cc-pVTZ-pp basis sets. The addition of a methyl group to the Cp ring in tellurium- and selenium-containing complexes results in an alteration of their atomic structure as well as their electronic properties. The dipole moment values of the complexes showed that the degree of polarity and ionic character is increased in the order of  $[\text{Cp}][(\text{TePh}_3)]$ ,  $[\text{Cp}^{\text{Me}4}][(\text{TePh}_3)]$ ,  $[\text{Cp}^{\text{Me}5}][(\text{TePh}_3)]$ ,  $[\text{Cp}][(\text{SePh}_3)]$ , and  $[\text{Cp}^{\text{Me}5}][(\text{SePh}_3)]$ , following the increase in the ionic character of the chemical bonding. A significant decrease was observed in the HOMO–LUMO gap for both  $[\text{Cp}^{\text{Me}4}][(\text{TePh}_3)]$  and  $[\text{Cp}^{\text{Me}5}][(\text{TePh}_3)]$ , and similarly for the selenium complexes  $[\text{Cp}][(\text{SePh}_3)]$  and  $[\text{Cp}^{\text{Me}5}][(\text{SePh}_3)]$ . The decrease in the HOMO–LUMO gap for these complexes could increase their chemical reactivity with a consequent decrease in their chemical stability. The major contribution to the LUMO of tellurium complexes comes from carbon atoms from  $\text{Ph}_3$  fragments, with visible percentages of density coming from the tellurium atom, which agrees well with the considerable shift observed in their visible light absorption. This study provides new insights into the structural, electronic, and optical properties of  $\eta^5$ -cyclopentadienyl half-sandwich Te and Se organochalcogenides complexes, which are promising for advanced photovoltaic and light-emitting applications. However, further experimental and theoretical investigations of the photoconductivity response, electronic transport, and recombination mechanism of these complexes would be significant for advanced optoelectronic applications.

**Supplementary Materials:** The following supporting information can be downloaded at: <https://www.mdpi.com/article/10.3390/electronics12122738/s1>, Table S1: Total energy (in a.u.) for Cp fragment (EF1),  $\text{EPh}_3$  fragments (EF2) and EP for  $[\text{Cp}][(\text{EPh}_3)]$ ; Atomic coordinates of all  $\eta^5$ -cyclopentadienyl half-sandwich organochalcogenides complexes optimized at ab initio TPSS/(cc-pVTZ-PP/6-31G\*) level of theory.

**Author Contributions:** Conceptualization, P.V.A. and I.A.M.; methodology, G.T.O., S.P.P. and I.A.M.; software, G.T.O.; validation, P.V.A. and S.P.P.; investigation, G.T.O. and I.A.M.; resources, P.V.A. and S.P.P.; writing—original draft preparation, G.T.O.; writing—review and editing, P.V.A., G.T.O., S.P.P. and I.A.M.; visualization, G.T.O.; supervision, P.V.A.; project administration, P.V.A. All authors have read and agreed to the published version of the manuscript.

**Funding:** Korean Team was supported by the National Research Foundation of the Republic of Korea, grant NRF 2021R1A2C1010455. Electronic structure calculations were supported by Project FSRZ-2023-0006 of the Ministry of Science and Higher Education of the Russian Federation.

**Data Availability Statement:** The data that support the findings of this study are available upon reasonable request from the corresponding authors.

**Acknowledgments:** The Korean team acknowledges the National Research Foundation of the Republic of Korea for its support under Grant NRF 2021R1A2C1010455. SFU IRC SQC team was supported by Project No. FSRZ-2023-0006 of the Ministry of Science and Higher Education of the Russian Federation. Iu.M. expresses gratitude to ITMO Fellowship program for the financial support.

**Conflicts of Interest:** Authors declare no conflict of interests.

#### References

1. Liu, S.-S.; Ziller, J.W.; Zhang, Y.-Q.; Wang, B.-W.; Evans, W.J.; Gao, S. A half-sandwich organometallic single-ion magnet with hexamethylbenzene coordinated to the Dy (III) ion. *Chem. Commun.* **2014**, *50*, 11418–11420. [[CrossRef](#)] [[PubMed](#)]
2. Lu, Y.; Zhang, H.-N.; Jin, G.-X. Molecular borromean rings based on half-sandwich organometallic rectangles. *Acc. Chem. Res.* **2018**, *51*, 2148–2158. [[CrossRef](#)] [[PubMed](#)]

3. Mészáros, J.P.; Pape, V.F.; Szakács, G.; Németi, G.; Dénes, M.; Holczbauer, T.; May, N.V.; Enyedy, É.A. Half-sandwich organometallic Ru and Rh complexes of (N, N) donor compounds: Effect of ligand methylation on solution speciation and anticancer activity. *Dalton Trans.* **2021**, *50*, 8218–8231. [[CrossRef](#)] [[PubMed](#)]
4. Natarajan, M.; Li, X.; Zhong, W.; Wang, W.; Xiao, Z.; Jiang, X.; Lu, C.; Liu, X. Three half-sandwiched iron (II) monocarbonyl complexes with PNP ligands: Their chemistry upon reduction and catalysis on proton reduction. *Electrochim. Acta* **2022**, *433*, 141207. [[CrossRef](#)]
5. Kisets, I.; Zabelinskaya, S.; Gelman, D. Synthesis and Catalytic Properties of a Carbometalated Half-Sandwich Ru (II) Complex Bearing a Rigid Polyaromatic Tether. *Organometallics* **2021**, *41*, 76–82. [[CrossRef](#)]
6. Pilia, L.; Shuku, Y.; Dagleish, S.; Hofmann, D.W.; Melis, N.; Awaga, K.; Robertson, N. Effect of fluorination on the crystal and electronic structure of organometallic cyclopentadienyl-phenylenediamino-cobalt complexes. *J. Organomet. Chem.* **2020**, *918*, 121277. [[CrossRef](#)]
7. Wang, Y.; Guo, W.; Guan, A.-L.; Liu, S.; Yao, Z.-J. Half-Sandwich Iridium Complexes Based on  $\beta$ -Ketoamino Ligands: Preparation, Structure, and Catalytic Activity in Amide Synthesis. *Inorg. Chem.* **2021**, *60*, 11514–11520. [[CrossRef](#)]
8. Avramov, P.; Sakai, S.; Naramoto, H.; Narumi, K.; Matsumoto, Y.; Maeda, Y. Theoretical DFT Study of Atomic Structure and Spin States of the  $\text{Co}_x(\text{C}_{60})_n$  ( $x=3-8, n=1, 2$ ) Complex Nanoclusters. *J. Phys. Chem. C* **2008**, *112*, 13932–13936. [[CrossRef](#)]
9. Avramov, P.; Naramoto, H.; Sakai, S.; Narumi, K.; Lavrentiev, V.; Maeda, Y. Quantum Chemical Study of Atomic Structure Evolution of  $\text{Co}_x/\text{C}_{60}$  ( $x \leq 2.8$ ) Composites. *J. Phys. Chem. A* **2007**, *111*, 2299–2306. [[CrossRef](#)]
10. Sakai, S.; Naramoto, H.; Avramov, P.V.; Yaita, T.; Lavrentiev, V.; Narumi, K.; Baba, Y.; Maeda, Y. Comparative study of structures and electrical properties in cobalt–fullerene mixtures by systematic change of cobalt content. *Thin Solid Film.* **2007**, *515*, 7758–7764. [[CrossRef](#)]
11. Sakai, S.; Yakushiji, K.; Mitani, S.; Sugai, I.; Takanashi, K.; Naramoto, H.; Avramov, P.V.; Lavrentiev, V.; Narumi, K.; Maeda, Y. Magnetic and magnetotransport properties in nanogranular Co/C<sub>60</sub>-Co film with high magnetoresistance. *Mater. Trans.* **2007**, *48*, 754–758. [[CrossRef](#)]
12. Banerjee, S.; Sadler, P.J. Transfer hydrogenation catalysis in cells. *RSC Chem. Biol.* **2021**, *2*, 12–29. [[CrossRef](#)]
13. Zhong, X.; Wang, H.; Zhang, J.; Liu, H.; Zhang, S.; Song, H.-F.; Yang, G.; Zhang, L.; Ma, Y. Tellurium hydrides at high pressures: High-temperature superconductors. *Phys. Rev. Lett.* **2016**, *116*, 057002. [[CrossRef](#)]
14. Huang, W.; Zhang, Y.; You, Q.; Huang, P.; Wang, Y.; Huang, Z.N.; Ge, Y.; Wu, L.; Dong, Z.; Dai, X. Enhanced photodetection properties of tellurium@ selenium roll-to-roll nanotube heterojunctions. *Small* **2019**, *15*, 1900902. [[CrossRef](#)]
15. Wang, L.; Cao, W.; Xu, H. Tellurium-containing polymers: Towards biomaterials and optoelectronic materials. *ChemNanoMat* **2016**, *2*, 479–488. [[CrossRef](#)]
16. Steinke, T.; Wonner, P.; Engelage, E.; Huber, S.M. Catalytic Activation of a Carbon–Chloride Bond by Dicationic Tellurium-Based Chalcogen Bond Donors. *Synthesis* **2021**, *53*, 2043–2050.
17. Sacramento, M.; Costa, G.P.; Barcellos, A.M.; Perin, G.; Lenardão, E.J.; Alves, D. Transition-Metal-Free C–S, C–Se, and C–Te Bond Formation from Organoboron Compounds. *Chem. Rec.* **2021**, *21*, 2855–2879. [[CrossRef](#)]
18. Singh, A.; Kaushik, A.; Dhau, J.S.; Kumar, R. Exploring coordination preferences and biological applications of pyridyl-based organochalcogen (Se, Te) ligands. *Coord. Chem. Rev.* **2022**, *450*, 214254. [[CrossRef](#)]
19. Ali, A.; Banerjee, B.; Srivastava, V.; Verma, V.K. Organochalcogen (Se/Te) substituted Schiff bases: Syntheses and applications. *Mater. Today Proc.* **2023**, *in press*. [[CrossRef](#)]
20. Zhou, J.; Qian, S.; Hao, B.; Liu, J.; Zhou, X.; Yan, C.; Qian, T. Small Molecules, Great Powers: Chemistry of Small Organochalcogenide Molecules in Rechargeable Li-Sulfur Batteries. *Adv. Funct. Mater.* **2023**, 2213966. [[CrossRef](#)]
21. Hassan, A.F.; Abdalwahed, A.T.; Al-Luaibi, M.Y.; Aljadaan, S.A. Synthesis, Characterization and Thermal Study of some new Organochalcogenide compounds containing arylamide group. *Egypt. J. Chem.* **2021**, *64*, 5009–5015. [[CrossRef](#)]
22. Kershaw, S.V.; Yiu, W.K.; Sergeev, A.; Rogach, A.L. Development of synthetic methods to grow long-wavelength infrared-emitting HgTe quantum dots in dimethylformamide. *Chem. Mater.* **2020**, *32*, 3930–3943. [[CrossRef](#)]
23. Patsha, A.; Ranganathan, K.; Kazes, M.; Oron, D.; Ismach, A. Halide chemical vapor deposition of 2D semiconducting atomically-thin crystals: From self-seeded to epitaxial growth. *Appl. Mater. Today* **2022**, *26*, 101379. [[CrossRef](#)]
24. Mane, R.; Mali, S.; Ghanwat, V.; Kondalkar, V.; Khot, K.; Mane, S.; Shinde, D.; Patil, P.; Bhosale, P. Photoelectrochemical Performance of MoBiInSe<sub>5</sub> Mixed Metal Chalcogenide Thin Films. *Mater. Today Proc.* **2015**, *2*, 1458–1463. [[CrossRef](#)]
25. Yeo, J.S.; Vittal, J.J.; Henderson, W.; Hor, T.A. Ligand functionalization, reactivity, and transformation at the selenide centers of [Pt<sub>2</sub>( $\mu$ -Se)<sub>2</sub>(PPh<sub>3</sub>)<sub>4</sub>] with organic halides. *Organometallics* **2002**, *21*, 2944–2949. [[CrossRef](#)]
26. Frogley, B.J.; Hill, A.F.; Watson, L.J. Bridging selenocarbonyl ligands: An open and shut case. *Chem. Commun.* **2019**, *55*, 14450–14453. [[CrossRef](#)]
27. Hesford, M.; Levason, W.; Orchard, S.D.; Reid, G. Synthesis and complexation of a new facultative tridentate S<sub>2</sub>Te donor ligand MeS(CH<sub>2</sub>)<sub>3</sub>Te(CH<sub>2</sub>)<sub>3</sub>SMe: Crystal structures of [Rh(Cp\*)(S<sub>2</sub>Te)][PF<sub>6</sub>]<sub>2</sub> and [PtCl(S<sub>2</sub>Te)]PF<sub>6</sub>. *J. Organomet. Chem.* **2002**, *649*, 214–218. [[CrossRef](#)]
28. Kieser, J.M.; Jones, L.O.; Uible, M.C.; Zeller, M.; Schatz, G.C.; Bart, S.C. Late to the Party: Synthesis and Characterization of Tellurium and Selenium Half-Sandwich Complexes. *Organometallics* **2021**, *40*, 4104–4109. [[CrossRef](#)]

29. Molonia, M.S.; Muscarà, C.; Speciale, A.; Salamone, F.L.; Toscano, G.; Saija, A.; Cimino, F. The p-Phthalates Terephthalic Acid and Dimethyl Terephthalate Used in the Manufacture of PET Induce In Vitro Adipocytes Dysfunction by Altering Adipogenesis and Thermogenesis Mechanisms. *Molecules* **2022**, *27*, 7645. [[CrossRef](#)]
30. Rusakov, Y.Y.; Rusakova, I.L. Long-range relativistic heavy atom effect on <sup>1</sup>H NMR chemical shifts of selenium-and tellurium-containing compounds. *Int. J. Quantum Chem.* **2019**, *119*, e25809. [[CrossRef](#)]
31. Pirillo, J.; De Simone, B.C.; Russo, N. Photophysical properties prediction of selenium-and tellurium-substituted thymidine as potential UVA chemotherapeutic agents. *Theor. Chem. Acc.* **2016**, *135*, 1–5. [[CrossRef](#)]
32. Rusakov, Y.Y.; Rusakova, I.L. Hierarchical basis sets for the calculation of nuclear magnetic resonance spin–spin coupling constants involving either selenium or tellurium nuclei. *J. Phys. Chem. A* **2019**, *123*, 6564–6571. [[CrossRef](#)]
33. Roca Jungfer, M.; Schulz Lang, E.; Abram, U. Solvents and Ligands Matter: Structurally Variable Palladium and Nickel Clusters Assembled by Tridentate Selenium-and Tellurium-Containing Schiff Bases. *Inorg. Chem.* **2022**, *61*, 3785–3800. [[CrossRef](#)]
34. Sharma, T.; Sharma, R.; Tamboli, R.A.; Kanhere, D.G. Ab initio investigation of structural and electronic properties of selenium and tellurium clusters. *Eur. Phys. J. B* **2019**, *92*, 1–14. [[CrossRef](#)]
35. Nagashima, Y.; Ishigaki, S.; Tanaka, J.; Tanaka, K. Acceleration Mechanisms of C–H Bond Functionalization Catalyzed by Electron-Deficient CpRh (III) Complexes. *ACS Catal.* **2021**, *11*, 13591–13602. [[CrossRef](#)]
36. Zakharov, A.V.; Sadekov, I.D.; Minkin, V.I. Synthesis, reactions and structures of telluronium salts. *Russ. Chem. Rev.* **2006**, *75*, 207. [[CrossRef](#)]
37. Günther, W.; Nepywoda, J.; Chu, J. Methods in chalcogen chemistry: V. A new reagent for the synthesis of aromatic tellurium compounds. *J. Organomet. Chem.* **1974**, *74*, 79–84. [[CrossRef](#)]
38. Abd-Elnaiem, A.M.; Abdelraheem, A.; Abdel-Rahim, M.; Moustafa, S. Substituting silver for tellurium in selenium–tellurium thin films for improving the optical characteristics. *J. Inorg. Organomet. Polym. Mater.* **2022**, *32*, 2009–2021. [[CrossRef](#)]
39. Abu-Sehly, A.; Rashad, M.; Hafiz, M.; Abd-Elmageed, A.; Amin, R. Tuning optical properties of thin films based on selenium tellurium. *Opt. Mater.* **2020**, *109*, 110291. [[CrossRef](#)]
40. Rashad, M.; Shaalan, N.; Abd-Elmageed, A.; Amin, R.; Hafiz, M.; Abu-Sehly, A. The effects of different dopant on the optical parameters for selenium tellurium thin films. *Optik* **2021**, *241*, 166102. [[CrossRef](#)]
41. Hadar, I.; Hu, X.; Luo, Z.-Z.; Dravid, V.P.; Kanatzidis, M.G. Nonlinear band gap tunability in selenium–tellurium alloys and its utilization in solar cells. *ACS Energy Lett.* **2019**, *4*, 2137–2143. [[CrossRef](#)]
42. Mondal, R.; Biswas, D.; Paul, S.; Das, A.S.; Chakrabarti, C.; Roy, D.; Bhattacharya, S.; Kabi, S. Investigation of microstructural, optical, physical properties and dielectric relaxation process of sulphur incorporated selenium–tellurium ternary glassy systems. *Mater. Chem. Phys.* **2021**, *257*, 123793. [[CrossRef](#)]
43. Barca, G.M.; Bertoni, C.; Carrington, L.; Datta, D.; De Silva, N.; Deustua, J.E.; Fedorov, D.G.; Gour, J.R.; Gunina, A.O.; Guidez, E. Recent developments in the general atomic and molecular electronic structure system. *J. Chem. Phys.* **2020**, *152*, 154102. [[CrossRef](#)] [[PubMed](#)]
44. Schmidt, M.W.; Baldridge, K.K.; Boatz, J.A.; Elbert, S.T.; Gordon, M.S.; Jensen, J.H.; Koseki, S.; Matsunaga, N.; Nguyen, K.A.; Su, S.; et al. General atomic and molecular electronic structure system. *J. Comput. Chem.* **1993**, *14*, 1347–1363. [[CrossRef](#)]
45. Becke, A.D. Density-functional exchange-energy approximation with correct asymptotic behavior. *Phys. Rev. A* **1988**, *38*, 3098. [[CrossRef](#)] [[PubMed](#)]
46. Tirado-Rives, J.; Jorgensen, W.L. Performance of B3LYP density functional methods for a large set of organic molecules. *J. Chem. Theory Comput.* **2008**, *4*, 297–306. [[CrossRef](#)]
47. Adamo, C.; Barone, V. Toward reliable density functional methods without adjustable parameters: The PBE0 model. *J. Chem. Phys.* **1999**, *110*, 6158–6170. [[CrossRef](#)]
48. Salavati-Niasari, M.; Mirsattari, S.; Monajjemi, M.; Hamadani, M. Density functional B3LYP and B3PW91 studies of the properties of four cyclic organodiboranes with tetramethylene fragments. *J. Struct. Chem.* **2010**, *51*, 437–443. [[CrossRef](#)]
49. Zhao, Y.; Truhlar, D.G. Density functional theory for reaction energies: Test of meta and hybrid meta functionals, range-separated functionals, and other high-performance functionals. *J. Chem. Theory Comput.* **2011**, *7*, 669–676. [[CrossRef](#)]
50. Kossmann, S.; Kirchner, B.; Neese, F. Performance of modern density functional theory for the prediction of hyperfine structure: Meta-GGA and double hybrid functionals. *Mol. Phys.* **2007**, *105*, 2049–2071. [[CrossRef](#)]
51. Wang, Y.; Verma, P.; Jin, X.; Truhlar, D.G.; He, X. Revised M06 density functional for main-group and transition-metal chemistry. *Proc. Natl. Acad. Sci. USA* **2018**, *115*, 10257–10262. [[CrossRef](#)]
52. Hohenstein, E.G.; Chill, S.T.; Sherrill, C.D. Assessment of the performance of the M05– 2X and M06– 2X exchange-correlation functionals for noncovalent interactions in biomolecules. *J. Chem. Theory Comput.* **2008**, *4*, 1996–2000. [[CrossRef](#)]
53. Hariharan, P.C.; Pople, J.A. The influence of polarization functions on molecular orbital hydrogenation energies. *Theor. Chim. Acta* **1973**, *28*, 213–222. [[CrossRef](#)]
54. Iyer, S.; Lopez-Hilfiker, F.; Lee, B.H.; Thornton, J.A.; Kurten, T. Modeling the detection of organic and inorganic compounds using iodide-based chemical ionization. *J. Phys. Chem. A* **2016**, *120*, 576–587. [[CrossRef](#)]
55. Karton, A. How reliable is DFT in predicting relative energies of polycyclic aromatic hydrocarbon isomers? comparison of functionals from different rungs of jacob’s ladder. *J. Comput. Chem.* **2017**, *38*, 370–382. [[CrossRef](#)]

56. Nakajima, Y.; Seino, J.; Nakai, H. Relativistic effect on enthalpy of formation for transition-metal complexes. *Chem. Phys. Lett.* **2017**, *673*, 24–29. [[CrossRef](#)]
57. Pritchard, B.P.; Altarawy, D.; Didier, B.; Gibson, T.D.; Windus, T.L. New basis set exchange: An open, up-to-date resource for the molecular sciences community. *J. Chem. Inf. Model.* **2019**, *59*, 4814–4820. [[CrossRef](#)]
58. Rassolov, V.A.; Ratner, M.A.; Pople, J.A.; Redfern, P.C.; Curtiss, L.A. 6-31G\* Basis Set for Third-Row Atoms. *J. Comp. Chem.* **2001**, *22*, 976–984. [[CrossRef](#)]
59. Xu, X.; Truhlar, D.G. Accuracy of effective core potentials and basis sets for density functional calculations, including relativistic effects, as illustrated by calculations on arsenic compounds. *J. Chem. Theory Comput.* **2011**, *7*, 2766–2779. [[CrossRef](#)]
60. Peterson, K.A.; Puzzarini, C. Systematically convergent basis sets for transition metals. II. Pseudopotential-based correlation consistent basis sets for the group 11 (Cu, Ag, Au) and 12 (Zn, Cd, Hg) elements. *Theor. Chem. Acc.* **2005**, *114*, 283–296. [[CrossRef](#)]
61. Bhattacharyya, M.; Prakash, R.; Nandi, C.; Chowdhury, M.G.; Raghavendra, B.; Roisnel, T.; Ghosh, S. Syntheses and structures of chalcogen-bridged binuclear group 5 and 6 metal complexes. *J. Chem. Sci.* **2019**, *131*, 1–13. [[CrossRef](#)]
62. Nakagawa, T.; Seino, H.; Mizobe, Y. Reactions of Bis (chalcogenolato) Complexes  $[\eta^5\text{-C}_5\text{Me}_5\text{Ir}(\text{CO})(\text{ETol})_2](\text{E}=\text{Se}, \text{S}; \text{Tol}=\text{p-Tolyl})$  with  $[\text{Pt}(\text{PPh}_3)_3]$ . Formation of Tri-or Dinuclear Mixed-Metal Complexes with Bridging Chalcogenido or Chalcogenolato Ligands. *Organometallics* **2010**, *29*, 2254–2259. [[CrossRef](#)]
63. Goerigk, L. A Comprehensive Overview of the DFT-D3 London-Dispersion Correction. In *Non-Covalent Interactions in Quantum Chemistry and Physics*; Elsevier: Cambridge, UK, 2017; pp. 195–219.
64. Smith, D.G.; Burns, L.A.; Patkowski, K.; Sherrill, C.D. Revised damping parameters for the D3 dispersion correction to density functional theory. *J. Phys. Chem. Lett.* **2016**, *7*, 2197–2203. [[CrossRef](#)] [[PubMed](#)]
65. Hoggan, P.E. *Proceedings of MEST 2012: Electronic Structure Methods with Applications to Experimental Chemistry*; Academic Press: Cambridge, MA, USA, 2014.
66. Liu, W.-K.; Kong, S.-S.; Yu, X.-X.; Li, Y.-L.; Yang, L.-Z.; Ma, Y.; Fang, X.-Y. Interlayer coupling, electronic and optical properties of few-layer silicon carbide nanosheets. *Mater. Today Commun.* **2023**, *34*, 105030. [[CrossRef](#)]
67. Kong, S.-S.; Liu, W.-K.; Yu, X.-X.; Li, Y.-L.; Yang, L.-Z.; Ma, Y.; Fang, X.-Y. Interlayer interaction mechanism and its regulation on optical properties of bilayer SiCNSs. *Front. Phys.* **2023**, *18*, 43302. [[CrossRef](#)]
68. Hao, P.; Sun, J.; Xiao, B.; Ruzsinszky, A.; Csonka, G.I.; Tao, J.; Glindmeyer, S.; Perdew, J.P. Performance of meta-GGA functionals on general main group thermochemistry, kinetics, and noncovalent interactions. *J. Chem. Theory Comput.* **2013**, *9*, 355–363. [[CrossRef](#)]
69. Wang, Y.; Jin, X.; Yu, H.S.; Truhlar, D.G.; He, X. Revised M06-L functional for improved accuracy on chemical reaction barrier heights, noncovalent interactions, and solid-state physics. *Proc. Natl. Acad. Sci. USA* **2017**, *114*, 8487–8492. [[CrossRef](#)]
70. Wang, G.-X.; Chen, W.; Yan, X.; Xie, F.; Wei, J.; Ye, S.; Xi, Z. Preparation and Characterization of a 19-Electron Ni (I) Complex Bearing a Cyclopentadienyl-Phosphine Ligand. *Organometallics* **2022**, *41*, 2227–2231. [[CrossRef](#)]
71. Silva, T.J.; Mendes, P.J.; Santos, A.M.; Garcia, M.H.; Robalo, M.P.; Ramalho, J.P.; Carvalho, A.P.; Büchert, M.; Wittenburg, C.; Heck, J.r. Mono ( $\eta^5$ -cyclopentadienyl) metal (II) complexes with thienyl acetylide chromophores: Synthesis, electrochemical studies, and first hyperpolarizabilities. *Organometallics* **2014**, *33*, 4655–4671. [[CrossRef](#)]
72. Bondi, A.v. van der Waals volumes and radii. *J. Phys. Chem.* **1964**, *68*, 441–451. [[CrossRef](#)]
73. Cotton, F.A.; Wilkinson, G.; Gaus, P.L. *Basic Inorganic Chemistry*; John Wiley & Sons: Hoboken, NJ, USA, 1995.
74. Miar, M.; Shiroudi, A.; Pourshamsian, K.; Oliaey, A.R.; Hatamjafari, F. Theoretical investigations on the HOMO–LUMO gap and global reactivity descriptor studies, natural bond orbital, and nucleus-independent chemical shifts analyses of 3-phenylbenzo [d] thiazole-2 (3 H)-imine and its para-substituted derivatives: Solvent and substituent effects. *J. Chem. Res.* **2021**, *45*, 147–158.
75. Li, G.; Chen, X.; Zhou, Z.; Wang, F.; Yang, H.; Yang, J.; Xu, B.; Yang, B.; Liu, D. Theoretical insights into the structural, relative stable, electronic, and gas sensing properties of  $\text{Pb}_n\text{Au}_n$  ( $n=2\text{--}12$ ) clusters: A DFT study. *RSC Adv.* **2017**, *7*, 45432–45441. [[CrossRef](#)]
76. Guo, Y.; Shi, W.; Zhu, Y. Internal electric field engineering for steering photogenerated charge separation and enhancing photoactivity. *EcoMat* **2019**, *1*, e12007. [[CrossRef](#)]
77. Coehoorn, R.; Lin, X.; Weijtens, C.; Gottardi, S.; Van Eersel, H. Three-Dimensional Modeling of Organic Light-Emitting Diodes Containing Molecules with Large Electric Dipole Moments. *Phys. Rev. Appl.* **2021**, *16*, 034048. [[CrossRef](#)]
78. Tzeli, D.; Petsalakis, I.D.; Theodorakopoulos, G.; Rahman, F.-U.; Yu, Y.; Rebek, J. The role of electric field, peripheral chains, and magnetic effects on significant  $^1\text{H}$  upfield shifts of the encapsulated molecules in chalcogen-bonded capsules. *Phys. Chem. Chem. Phys.* **2021**, *23*, 19647–19658. [[CrossRef](#)]
79. Thomas, A.A.; Speck, K.; Kevlishvili, I.; Lu, Z.; Liu, P.; Buchwald, S.L. Mechanistically guided design of ligands that significantly improve the efficiency of CuH-catalyzed hydroamination reactions. *J. Am. Chem. Soc.* **2018**, *140*, 13976–13984. [[CrossRef](#)]
80. Cui, C.-H.; Yu, S.-H. Engineering interface and surface of noble metal nanoparticle nanotubes toward enhanced catalytic activity for fuel cell applications. *Acc. Chem. Res.* **2013**, *46*, 1427–1437. [[CrossRef](#)]

81. Li, H.H.; Yu, S.H. Recent advances on controlled synthesis and engineering of hollow alloyed nanotubes for electrocatalysis. *Adv. Mater.* **2019**, *31*, 1803503. [[CrossRef](#)]
82. Yang, Y.-Y.; Gong, P.; Ma, W.-D.; Hao, R.; Fang, X.-Y. Effects of substitution of group-V atoms for carbon or silicon atoms on optical properties of silicon carbide nanotubes. *Chin. Phys. B* **2021**, *30*, 067803. [[CrossRef](#)]

**Disclaimer/Publisher's Note:** The statements, opinions and data contained in all publications are solely those of the individual author(s) and contributor(s) and not of MDPI and/or the editor(s). MDPI and/or the editor(s) disclaim responsibility for any injury to people or property resulting from any ideas, methods, instructions or products referred to in the content.